www.czasopisma.pan.pl PAN POLSKA AKADEMIA NAUK www.journals.pan.pl

A R C H I V E S O F M E T A L L U R G Y A N D M A T E R I A L S

Volume 60 2015 Issue 1

DOI: 10.1515/amm-2015-0001

K. BŁOCH*, M. NABIAŁEK*, M. DOŚPIAŁ*, S. GARUS*

CRYSTALLIZATION OF Fe-BASED BULK AMORPHOUS ALLOYS

KRYSTALIZACJA MASYWNYCH STOPÓW AMORFICZNYCH NA BAZIE ŻELAZA

The aim of this paper is to present the results of crystallization studies for the bulk amorphous $(Fe_{0.61}Co_{0.10}Zr_{0.025}Hf_{0.025}Ti_{0.02}W_{0.02}B_{0.20})_{98}Y_2$, $Fe_{61}Co_{10}Ti_xY_6B_{20}$, $Fe_{61}Co_{10}Ti_2Y_7B_{20}$ alloys. The crystallization of the alloys was studied by differential scanning calorimetry (DSC). The amorphicity of the investigated alloys in the as-quenched state was testified using Mössbauer spectroscopy, X-ray diffractometry and transmission electron microscopy. Moreover, X-ray diffractometry was applied to structure investigations of partially crystallized samples. The crystallization process in the investigated alloys occurs in one or two stages. Two peaks in the DSC curves can be overlapped or well separated indicating the complex crystallization processes. From X-ray diffraction we have stated that in both types of devitrification the crystalline phase can be ascribed to the α-FeCo. In the first stage the crystalline grains seem to grow from the nuclei frozen in the samples during the rapid quenching, whereas in the second one both the growth of the existed grains and creation of new ones during annealing may occur.

Keywords: bulk amorphous alloys, differential scanning calorimetry (DSC), X-ray diffractometry, transmission electron microscopy, Mössbauer spectroscopy

W pracy przedstawiono wyniki badań krystalizacji masywnych stopów amorficznych $(Fe_{0,61}Co_{0,10}Zr_{0,025}Hf_{0,025}Ti_{0,02}W_{0,02}B_{0,20})_{98}Y_2$, $Fe_{61}Co_{10}Ti_3Y_6B_{20}$, $Fe_{61}Co_{10}Ti_2Y_7B_{20}$ w postaci prętów. Krystalizację tych stopów badano wykorzystując skaningowy kalorymetr różnicowy (DSC). Amorficzność próbek w stanie po zestaleniu została zbadana przy użyciu spektroskopii Mössbauera, dyfrakcji promieni Röntgena oraz transmisyjnej mikroskopii elektronowej. Ponadto, dyfrakcję promieni X użyto do badań próbek częściowo skrystalizowanych. Na podstawie badań z wykorzystaniem DSC stwierdzono, że krystalizacja może przebiegać w jednym lub w dwóch etapach. Piki na krzywych DSC odpowiadające tym dwóm etapom mogą być położone blisko siebie lub wyraźnie rozdzielone. Pierwsze maksimum odpowiada tworzeniu się ziaren α-FeCo z zarodków powstałych podczas produkcji stopu, drugie natomiast związane jest z procesem tworzenia się ziaren fazy krystalicznej α-FeCo z zarodków powstałych podczas wygrzewania i rozrostem wcześniej powstałych ziaren.

1. Introduction

Iron-based amorphous ferromagnetic alloys have attracted much attention due to their great potential application and low material cost [1-3]. Conventional amorphous alloys are usually prepared by rapidly quenching of a molten material on a rotating wheel at cooling rate of the order of 10^6 K s^{-1} and have a shape of thin ribbons with thickness of about 40 μm. The packing density of the material in magnetic cores is low because of air gaps between layers. Multicomponent systems enable to produce amorphous materials at relatively low cooling rate of 1-10^2 K s^{-1} in the form of rods, tubes and thick ribbons [4-7]. One of the important parameters, which determine the application of amorphous material, is the thermal stability of the structure and magnetic properties. Instability of the amorphous alloys, connected with irreversible structure relaxations, leads to their crystallization at high temperature. We may distinguish two types of amorphous alloys [8,9]. Type one devitrifies directly to the crystalline phase. Whereas in the second type at first the quasicrystalline state is created and then during further heating it transforms to crystalline state [10-11].

The aim of this paper is to present the results of crystallization studies of the bulk amorphous $(Fe_{0.61}Co_{0.10}Zr_{0.025}Hf_{0.025}Ti_{0.02}W_{0.02}B_{0.20})_{98}Y_2$, $Fe_{61}Co_{10}Ti_3Y_6B_{20}$, $Fe_{61}Co_{10}Ti_2Y_7B_{20}$ alloys.

2. Experimental procedure

Alloy ingots with nominal composition $(Fe_{0.61}Co_{0.10}Zr_{0.025}Hf_{0.025}Ti_{0.02}W_{0.02}B_{0.20})_{98}Y_2$, $Fe_{61}Co_{10}Ti_3Y_6B_{20}$, $Fe_{61}Co_{10}Ti_2Y_7B_{20}$ were prepared by arc melting of high purity elements in an argon protective atmosphere. Each ingot was remelted four times to obtain the homogenous material. Amorphous rods 1 mm in diameter and 20 mm long (Fig. 1.) were obtained by a suction-casting method of the molten alloy into a copper mould cooled with water [12].

* INSTITUTE OF PHYSICS, CZESTOCHOWA UNIVERSITY OF TECHNOLOGY, 19 ARMII KRAJOWEJ AV., 42-200 CZESTOCHOWA, POLAND

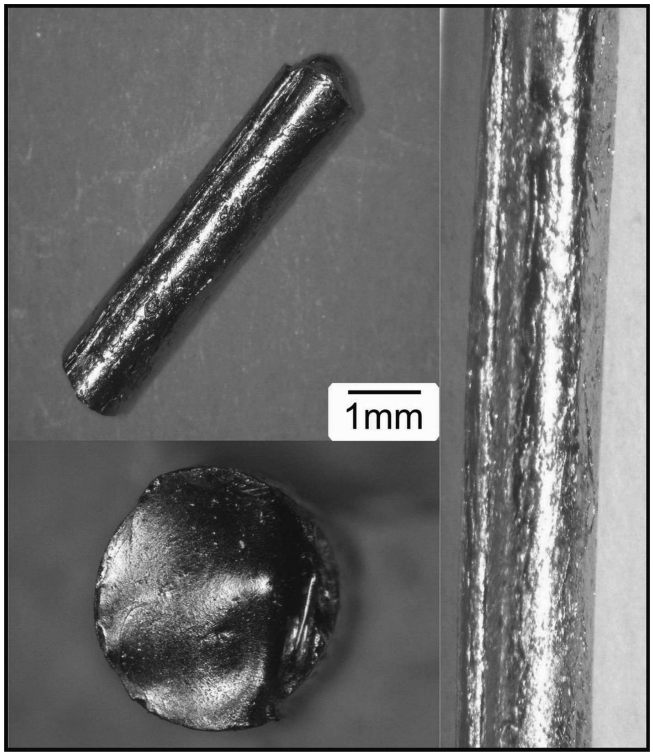

Fig. 1. Sight of amorphous rods obtained by an optical microscope

The structure of the samples was investigated using Mössbauer spectroscopy, X-ray diffractometry and transmission electron microscopy. The Mössbauer spectrum and X-ray diffractions patterns were measured for powdered samples. The crystallization of the alloys was studied by differential scanning calorimetry (DSC) for the samples in the form of rods and after powdering. The heat treatment of the samples was carried out in an argon atmosphere using a differential scanning calorimeter.

3. Results and discussion

In the Fig. 2 X-ray diffractions patterns for as-received $(Fe_{0.61}Co_{0.10}Zr_{0.025}Hf_{0.025}Ti_{0.02}W_{0.02}B_{0.20})_{98}Y_2$, $Fe_{61}Co_{10}Ti_3Y_6B_{20}$, $Fe_{61}Co_{10}Ti_2Y_7B_{20}$ alloys are presented.

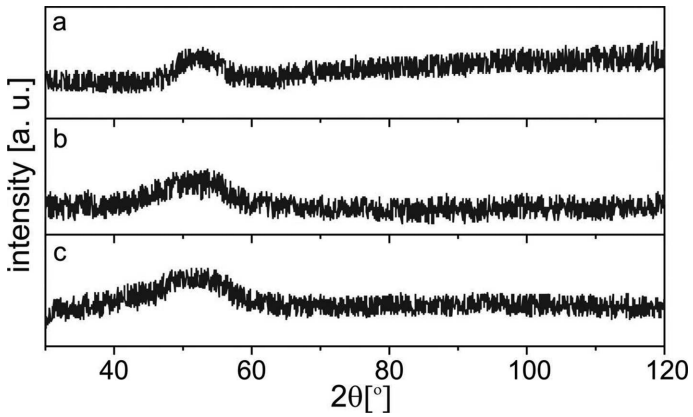

Fig. 2. XRD patterns obtained for as-received powdered samples (a) – $(Fe_{0.61}Co_{0.10}Zr_{0.25}Hf_{0.25}Ti_{0.02}W_{0.02}B_{0.2})_{98}Y_2$, (b) – $Fe_{61}Co_{10}Ti_3Y_6B_{20}$, (c) – $Fe_{61}Co_{10}Ti_2Y_7B_{20}$

X-ray diffraction patterns are characteristic of the amorphous state and consist of broad maxima. No narrow peaks typical of crystalline phases are present.

Transmission Mössbauer spectra and obtained from them hyperfine field induction distributions for the same samples are shown in Fig. 3.

Mössbauer spectra are typical of amorphous alloys and have the form of sextet with broad and overlapped lines. The hyperfine induction distributions do not exhibit the unimodal character and we may distinguished in them at least two components corresponding to the different environment of ^{57}Fe atoms.

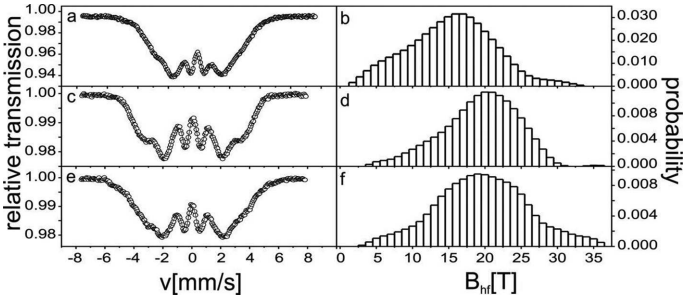

Fig. 3. Transmission Mössbauer spectra (a, b, c) and corresponding hyperfine field induction distributions (d, e, f) for amorphous powdered alloys after preparation: (a, d) – $(Fe_{0.61}Co_{0.10}Zr_{0.025}Hf_{0.025}Ti_{0.02}W_{0.02}B_{0.20})_{98}Y_2$, (b, e) – $Fe_{61}Co_{10}Ti_3Y_6B_{20}$, (c, f) – $Fe_{61}Co_{10}Ti_2Y_7B_{20}$

The amorphous structure of the as-received alloys was also confirmed by transmission electron microscopy working at high resolution mode (HREM). In Fig. 4 the bright-field HREM-image for the sample of $(Fe_{0.61}Co_{0.10}Zr_{0.025}Hf_{0.025}Ti_{0.02}W_{0.02}B_{0.20})_{98}Y_2$ alloy, as an example, is depicted.

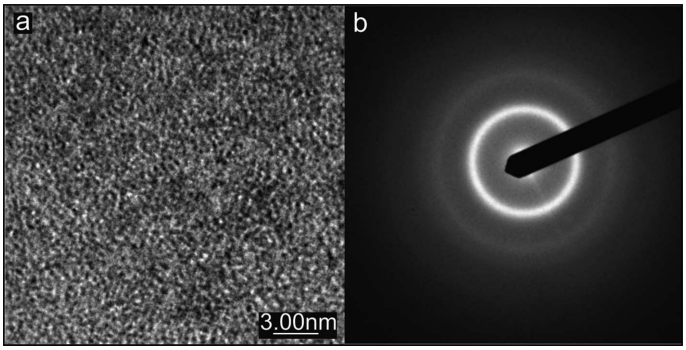

Fig. 4. Bright-field HREM-image (a) and corresponding electron diffraction pattern (b) obtained for the as-received $(Fe_{0.61}Co_{0.10}Zr_{0.025}Hf_{0.025}Ti_{0.02}W_{0.02}B_{0.20})_{98}Y_2$ alloy

In bright-field image no crystalline phases are observed and corresponding selected area diffraction pattern has form of a halo ring characteristic of an amorphous phase.

Fig. 5. shows DSC tracers obtained for small pieces (5 mm long) cut out from the as-quenched rods.

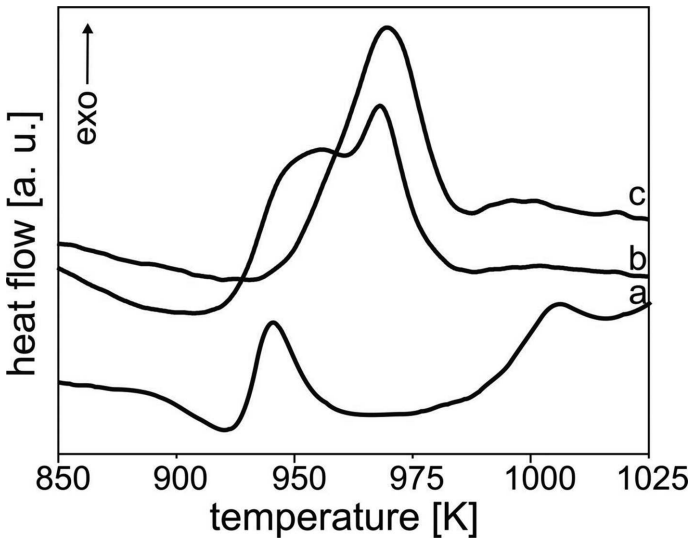

Fig. 5. DSC curves of as-received (a) – $(Fe_{0.61}Co_{0.10}Zr_{0.25}Hf_{0.25}Ti_{0.02}W_{0.02}B_{0.20})_{98}Y_2$, (b) – $Fe_{61}Co_{10}Ti_3Y_6B_{20}$, (c) – $Fe_{61}Co_{10}Ti_2Y_7B_{20}$ alloys recorded at heating rate of 10 K min^{-1}

DSC curve obtained for the amorphous $Fe_{61}Co_{10}Ti_2Y_7B_{20}$ alloy exhibits one exothermic peak at 969 K corresponding to the crystallization of the sample. As for the amorphous $Fe_{61}Co_{10}Ti_3Y_6B_{20}$ sample in the DSC curve we may distinguish near situated two peaks, one at 955 K and the second at 968 K. Well separated two peaks are observed in DSC curve for $(Fe_{0.61}Co_{0.10}Zr_{0.25}Hf_{0.25}Ti_{0.02}W_{0.02}B_{0.20})_{98}Y_2$, at 913 K and 998 K, respectively. DSC results indicate that the crystallization process in the latter two alloys occurs in two stages.

It is well known that it is thermally activated and the location of the peaks in DSC curves depends on the heating rate (Fig. 6).

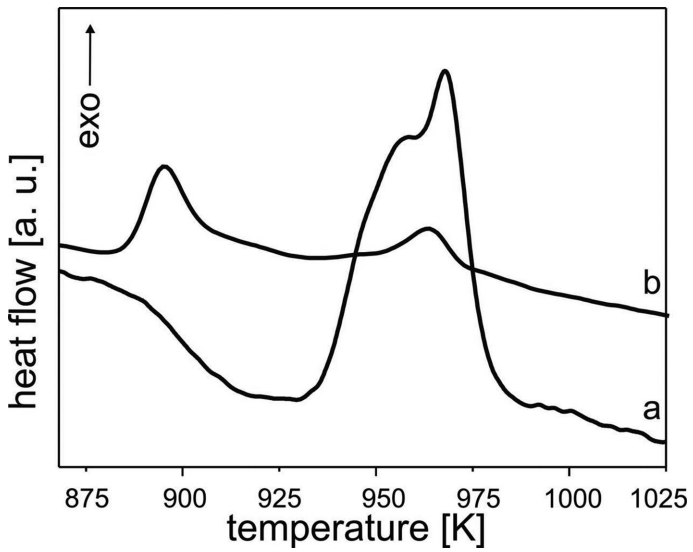

Fig. 6. Isochronal DSC curves recorded at heating rate 10 K min^{-1} (a) and 5 K min^{-1} (b) for the amorphous $Fe_{61}Co_{10}Ti_3Y_6B_{20}$ alloy

It is worth noticing that the first peak in the DSC curves measured at the heating rate of 5 K min^{-1} shifts from 957 K to 895 K, while the location of the second peak remains practically unchanged in comparison with curves recorded at 10 K min^{-1}.

DSC curves recorded at heating rate of 10 K min^{-1} for amorphous rods and powdered samples are presented in Fig. 7.

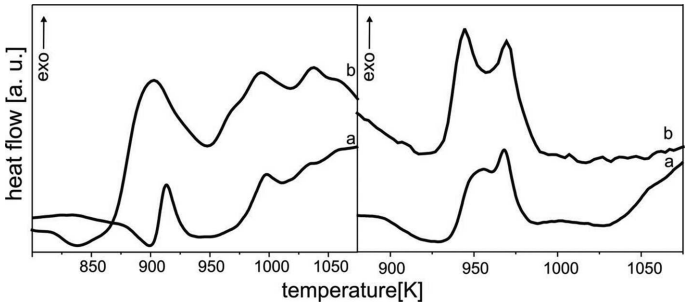

Fig. 7. DSC curves measured at the heating rate of 10 K min^{-1} for the bulk amorphous (A) $(Fe_{0.61}Co_{0.10}Zr_{0.025}Hf_{0.025}Ti_{0.02}W_{0.02}B_{0.20})_{98}Y_2$, (B) $Fe_{61}Co_{10}Ti_3Y_6B_{20}$, alloys: (a) – the samples in the form of the rod; (b) – powdered rod

The peaks in the DSC curves obtained for powdered samples are more pronounced and slightly shifted to lower temperature than for rods. It is connected with temperature distribution in the cross-section of rods during measurements of DSC curves.

In order to determine the phase composition of the samples in different stages of crystallization, X-ray diffraction patterns were measured for the samples in the proper stage of crystallization. In Fig. 8 DSC curves for the amorphous powdered $(Fe_{0.61}Co_{0.10}Zr_{0.025}Hf_{0.025}Ti_{0.02}W_{0.02}B_{0.20})_{98}Y_2$ sample measured in the temperature range from 800 K up to 920 K and from 800 K up to 1010 K and X-ray diffraction patterns recorded after breaking heat treatment at 920 K and 1010 K are shown.

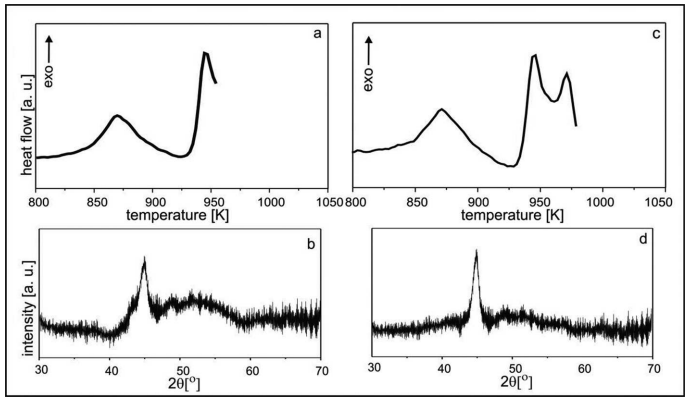

Fig. 8. DSC curves measured in the temperature range from 800 K up to 920 K (a) and from 800 K up to 1010 K (c) and X-ray diffraction patterns recorded after breaking heat treatment at 920 K (b) and 1010 K (d) for the amorphous powdered $(Fe_{0.61}Co_{0.10}Zr_{0.025}Hf_{0.025}Ti_{0.02}W_{0.02}B_{0.20})_{98}Y_2$ alloy

The X-ray diffractograms show the narrow peaks at 2θ = 44,8° corresponding to the crystalline phase. The intensity of this peak in X-ray pattern obtained for the sample is higher after the second stage of crystallization. The similar results were obtained for the bulk amorphous $Fe_{61}Co_{10}Ti_3Y_6B_{20}$ alloy (Fig. 9).

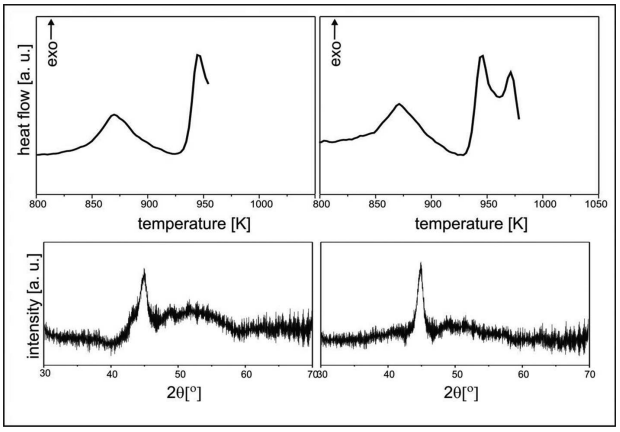

Fig. 9. DSC curves measured in the temperature range from 800 K up to 955 K (a) and from 800 K up to 980 K (c) and X-ray diffraction patterns recorded after breaking heat treatment at 955 K (b) and 980 K (d) for the amorphous powdered $Fe_{61}Co_{10}Ti_3Y_6B_{20}$ sample

The first peak observed in DSC curves for $(Fe_{0.61}Co_{0.10}Zr_{0.025}Hf_{0.025}Ti_{0.02}W_{0.02}B_{0.20})_{98}Y_2$ and $Fe_{61}Co_{10}Ti_3Y_6B_{20}$ alloys corresponds to creation of crystalline grains from nuclei quenched in during alloys preparation. However, the second peak is connected with the growth of existing grains and nuclei which were created during heating. DSC curve and X-ray diffraction pattern of the amorphous $Fe_{61}Co_{10}Ti_2Y_7B_{20}$ alloy are showed in Fig. 10.

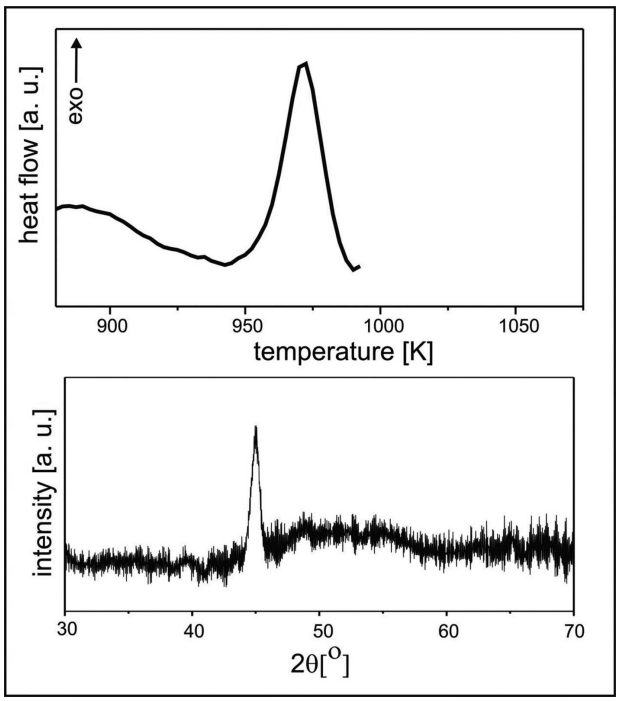

Fig. 10. DSC curve (a) measured in the temperature range from 800 K up to 990 K at the heating rate of 10 K min^{-1} and X-ray diffraction pattern (b) recorded after breaking heat treatment at 990 K for the amorphous powdered $Fe_{61}Co_{10}Ti_2Y_7B_{20}$ sample

DSC curve obtained for this alloy exhibits only one maximum. From the analysis of X-ray diffraction patterns it has been stated that during crystallization of the investigated alloys α-FeCo phase appears.

4. Conclusions

We found that the crystallization process of bulk amorphous alloys strongly depends on their chemical composition. The amorphous $(Fe_{0.61}Co_{0.10}Zr_{0.025}Hf_{0.025}Ti_{0.02}W_{0.02}B_{0.20})_{98}Y_2$ alloy crystallizes in two stages with well separated temperature. DSC curve for $Fe_{61}Co_{10}Ti_3Y_6B_{20}$ alloy shows near situated peaks, whereas the crystallization process for $Fe_{61}Co_{10}Ti_2Y_7B_{20}$ alloy takes place in one stage.

REFERENCES

[1] A. Inoue, Stabilization of metallic supercooled liquid and bulk amorphous alloys. Acta Mater. **48**, 279-306 (2000).

[2] C.Y. Lin, T.S. Chin, Soft magnetic (Fe, M)-Y-B(M = Co or Ni) bulk magnetic glasses. J. Alloys Compd **437**, 191-196 (2007).

[3] K. Sobczyk, J. Swierczek, J. Gondro, J. Zbroszczyk, W.H. Ciurzyńska, J. Olszewski, P. Brągiel, M. Nabiałek, Microstructure and some magnetic properties of bulk amorphous $(Fe_{0.61}Co_{0.10}Zr_{0.025}Hf_{0.025}Ti_{0.02}W_{0.02}B_{0.20})_{100-x}Y_x$ (x=0, 2, 3 or 4) alloys, J. Magn. Magn. Mater. **324** (4), 540-549 (2012).

[4] A. Inoue, Bulk amorphous alloys: Preparation and fundamental characteristic. Mater. Sci. Fundations 6, Trans Tech Publications, 1-116 (1998).

[5] J. Zbroszczyk, J. Olszewski, W. Ciurzyńska, M. Nabiałek, P. Pawlik, M. Hasiak, A. Łukiewska, K. Perduta, Glass-forming ability and magnetic properties of bulk $Fe_{61}Co_{10}Zr_{2.5}Hf_{2.5}W_{4-y}Me_yB_{20}$ (y = 0 or 2, Me = Mo, Ti) alloys. J. Magn. Magn. Mater. **304**, 724-726 (2006).

[6] A. Łukiewska, J. Zbroszczyk, M. Nabialek, J. Olszewski, J. Swierczek, W. Ciurzyńska, K. Sobczyk, M. Dospial, Low and high magnetic field properties of nanocrystalline $Fe_{59}Co_{15}Zr_2Y_4Nb_5B_{15}$ rods, Arch. Metall. Mater. **53 (3)**, 881-886 (2008).

[7] J. Zbroszczyk, P. Brągiel, M. Nabiałek, W.H. Ciurzyńska, J. Swierczek, A. Łukiewska, K. Sobczyk, Microstructure and magnetic behaviour of bulk amorphous $(Fe_{0.61}Co_{0.10}Zr_{0.025}Hf_{0.025}Ti_{0.02}W_{0.02}B_{0.20})_{100-x}Y_x$ (x = 0 or 2) alloys, J. Phys.: Conf. Ser. **79**, 012029 (2007).

[8] Z.M. Stadnik, Ö. Rapp., V. Srinivas, J. Saida, A. Inoue, Mössbauer and transport studies of amorphous and icosahedral Zr-Ni-Cu-Ag-Al alloys. J. Phys.: Condens. Matter **14**, 6883-6896 (2002).

[9] H. Bińczycka, S. Schneider, P. Schaff, Mössbauer effect and x-ray diffraction study of Zr-Ti-Cu-Ni-Be bulk metallic glasses. J. Phys.: Condens. Matter **15 (6)**, 945-955 (2003).

[10] R.C. O'Handley, Physics of ferromagnetic amorphous alloys. J. Appl. Phys. **62**, R15-R49 (1987).

[11] J. Gondro, J. Zbroszczyk, W. Ciurzyńska, J. Olszewski, M. Nabiałek, K. Sobczyk, J. Swierczek, A. Łukiewska, Structure and soft magnetic properties of bulk amorphous $(Fe_{0.61}Co_{0.10}Zr_{0.025}W_{0.02}Hf_{0.025}Ti_{0.02}B_{0.20})_{96}Y_4$ alloy, Arch. Metall. Mater. **55 (1)**, 85-90 (2010).

[12] J. Olszewski, J. Zbroszczyk, M. Hasiak, J. Kaleta, M. Nabiałek, P. Bragiel, K. Sobczyk, A. Łukiewska, Microstructure and magnetic properties of Fe-Co-Nd-Y-B alloys obtained by suction casting method, J. Rare Earths **27 (4)**, 680-683 (2009).

Received: 20 March 2014.